



Optimization of desert lake information extraction from remote sensing images using cellular automata

Qiuji Chen¹ · Yanan Cao¹

Received: 5 June 2022 / Revised: 10 December 2022 / Accepted: 13 June 2023
© The Author(s) 2023

Abstract

Desert lakes are important wetland resources in the blown-sand area of western China and play a significant role in maintaining the regional ecological environment. However, large-scale coal mining in recent years has considerably impacted the deposition condition of several lakes. Rapid and accurate extraction of lake information based on satellite images is crucial for developing protective measures against desertification. However, the spatial resolution of these images often leads to mixed pixels near water boundaries, affecting extraction precision. Traditional pixel unmixing methods mainly obtain water coverage information in a mixed pixel, making it difficult to accurately describe the spatial distribution. In this paper, the cellular automata (CA) model was adopted in order to realize lake information extraction at a sub-pixel level. A mining area in Shenmu City, Shaanxi Province, China is selected as the research region, using the image of Sentinel-2 as the data source and the high spatial resolution UAV image as the reference. First, water coverage of mixed pixels in the Sentinel-2 image was calculated with the dimidiate pixel model and the fully constrained least squares (FCLS) method. Second, the mixed pixels were subdivided to form the cellular space at a sub-pixel level and the transition rules are constructed based on the water coverage information and spatial correlation. Lastly, the process was implemented using Python and IDL, with the ArcGIS and ENVI software being used for validation. The experiments show that the CA model can improve the sub-pixel positioning accuracy for lake bodies in mixed pixel image and improve classification accuracy. The FCLS-CA model has a higher accuracy and is able to identify most water bodies in the study area, and is therefore suitable for desert lake monitoring in mining areas.

Keywords Blown-sand mining area · Desert lake · Remote sensing · Mixed pixel · Cellular automata

1 Introduction

The western blown-sand area in China is becoming the main coal-producing base. This area has several small desert lakes, which not only supply water for plants in sandy areas, but also serve as the main water source of surrounding residents and agriculture. Therefore, they play an important role in protecting the ecosystem of the blown-sand area. In recent years, large scale mining activities have caused a sharp decline in the number and area of desert lakes (Liu et al. 2017; Nie et al. 2018; Wang et al. 2020; Xu et al. 2019a, b; Zheng et al. 2021). Reducing the impact of coal mining on the fragile ecosystem, especially the desert

lakes, has become a problem that needs to be solved urgently at present. Therefore, obtaining the lake information accurately and rapidly is of great significance for the ecological environment protection and sustainable development in the mining area.

The development of remote sensing technology offers a promising tool for desert lake monitoring as it has outstanding advantages compared with traditional ground observation methods. The water area, water quality and other parameters can be obtained based on the optical remote sensing images (Ma et al. 2018; Wang et al. 2019a, b; Zhang et al. 2021a, b; Zhou and Dong 2019; Zhou et al. 2004). The extraction methods mainly include the threshold method, classifier method, object-oriented method, data mining method, water body index method, etc. (Jiang et al. 2011; Li et al. 2020; Liu 2020; Qiao and Sun 2020; Su et al. 2021; Wang et al. 2019a, b; Zhang et al. 2021a, b).

✉ Qiuji Chen
Qiujiichen@163.com

¹ College of Geomatics, Xi'an University of Science and Technology, Xi'an 710054, China

Among these methods, the water body index method is the most widely used one. It involves the formulation of a mathematical model of the water index through the selection of the bands closely related to the water body to enhance the contrast between the water body and the background, and then realize the rapid extraction of the water information (Zhang et al. 2022). Commonly used water body indices mainly include the normalized difference water index (NDWI), the modified NDWI (MNDWI), the automatic water extraction index (AWEI), and others. The NDWI is based on the spectral characteristics of water and surrounding vegetation in the near-infrared and green bands and can be used to extract water information from the image. The MNDWI uses the mid-infrared band to replace the near-infrared band to mitigate the influence of buildings when extracting water information within urban environments. The AWEI integrates the blue, green, near-infrared, short-wave infrared and mid-infrared band to construct a water index and inhibit the influence of shadows and buildings (Xu 2005; Feyisa et al. 2014).

Due to the limited spatial resolution of the remote sensing images, small lake areas and shallow water bodies, there are many mixed pixels near the water boundaries in the images, which affect the extraction precision.

In order to solve the problem of mixed pixels, researchers concentrating on feasible methods for mixed pixels in remote sensing images have developed a variety of spectral unmixing methods (Chen et al. 2016; Chen and Vierling 2006; Fan et al. 2009; Li et al. 2008, 2009, 2020; Wu 2004). Cui et al. (2019) combined decision tree and linear spectral unmixing methods to extract bamboo forest information in China. Yang et al. (2010) proposed an image unmixing method based on the posterior probability of relevance vector machines. Zhang et al. (2019) analyzed the factors influencing the decomposition precision of mixed pixels based on the constraint linear spectral mixing model. Liu et al. (2008) proposed a method for decomposing mixed pixels that combined self-organizing map (SOM) neural networks and fuzzy membership in the fuzzy theory. Li et al. (2016) presented a nonlinear spectral unmixing for optimizing per-pixel end member sets. Kong and Chen (2017) used the fully constrained least squares (FCLS) method to extract different reservoir surface water information.

Most of the traditional unmixing methods use spectral information to calculate the coverage of water bodies in a mixed pixel (Lai et al. 2019; Wang et al. 2008). However, it is difficult to describe the water spatial distribution state in the mixed pixel due to ignoring the spatial correlation information of the ground features, which affects the accuracy of lake information extraction.

The cellular automata model (CA) can be used in a sub-pixel level for the analysis of remote sensing images (Li et al. 2015). Feng and Han (2012) used CA to study the spatial distribution of coastlines using remote sensing images. Gao and Dai (2020) simulated water pollution dispersion based on improved CA model.

This paper selects a mining area in the Shenmu City, ShaanXi Province, China, as the research region. It uses the Sentinel-2 images as the data source and the high spatial resolution UAV images as the reference. The lake information extraction at a sub-pixel level is achieved by combining the dimidiate pixel model and FCLS with the CA model. This method not only considers the image spectral information, but also makes full use of the water body spatial correlation. Consequently, it can improve the accuracy of remote sensing image recognition and classification.

The remainder of the paper is organized as follows. In Sect. 2, the natural geographical conditions and the main data sets used in this study are described. Study methods are described in Sect. 3. The experimental process and accuracy analysis are presented in Sect. 4. A summary of the main conclusions and prospects of the research detailed in the paper is discussed in Sect. 5.

2 Study area and data processing

2.1 Overview of the study area

The study area is situated on the southeast edge of Maousu Desert at a distance of about 47 km from the Shenmu City, Shaanxi Province, China. It is in the arid to semi-arid transition zone of temperate continental monsoon climate and has the characteristics of drought, low rainfall and high annual evaporation. The surface is largely covered by quaternary blown-sand in the form of semi-fixed and fixed dunes. The ground elevation is between 1325.60 and 1234.10 m, with a relative maximum height difference of 91.50 m.

The surface water in the study area is mainly comprised of small lakes and the water storage volume changes in different seasons. The water depth is associated with geographical morphology, mostly between 0.3 and 5.0 m. The surface vegetation is mainly sandy vegetation. Figure 1 shows the desert lakes and surrounding environments.

2.2 Data acquisition and preprocessing

The remote sensing data for this experiment are based on the Sentinel-2 image that was acquired on 5 October 2020. It is downloaded from the Copernicus Open Access Hub

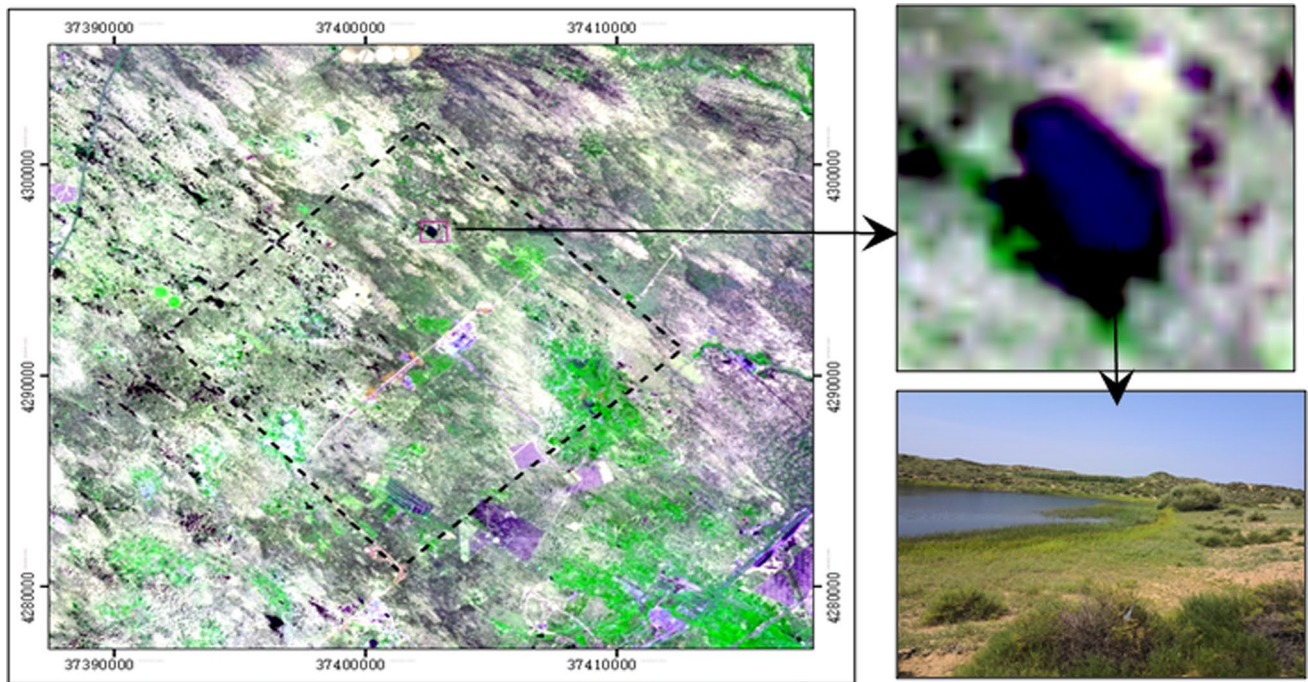


Fig. 1 Study area and photos of desert lakes

Table 1 Some bands information of Sentinel-2 image

Band number	Band name	Central wave-length (nm)	Spatial resolution (m)	Band number	Band name	Central wave-length (nm)	Spatial resolution (m)
B2	Blue	492.7	10	B7	Red Edge 3	782.8	20
B3	Green	559.8	10	B8	NIR	832.8	10
B4	Red	664.6	10	B11	SWIR	1613.7	20

(<https://scihub.copernicus.eu/>) and the product level is L2A, which has been passed through radiation calibration and atmospheric correction. The Sentinel-2 images have 13 bands with different spatial resolutions of 10, 20 and 60 m. Table 1 provides detailed information about the bands of Sentinel-2 images.

In order to verify the correctness of the proposed method, a UAV at a flight altitude of 80 m is used to collect high resolution images of the lake. The data qualities of these aerial images are first checked, and the images with relatively poor quality are removed. The remaining images are imported into the PhotoScan software to carry out image matching, aerial triangulation and irregular triangle network model construction, subsequently generating dense point clouds and a 3D model to obtain a Digital Orthophoto Map (DOM) with a spatial resolution of 0.02 m (Fig. 2), then some samples of lakes are obtained with a supervised method using the ENVI software as a reference for accuracy evaluation (Fig. 3).



Fig. 2 DOM of UAV

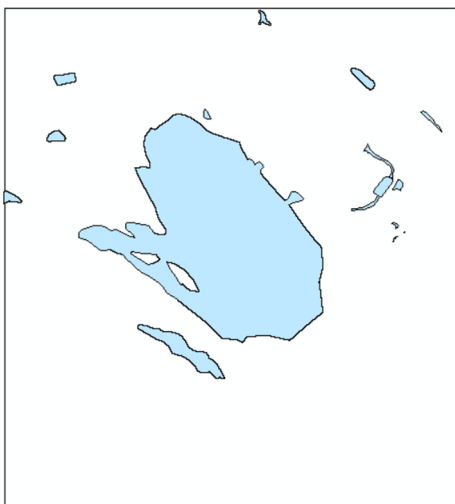


Fig. 3 Lake samples

3 Study methods

3.1 Water coverage index calculation based on dimidiate pixel (DP) model

When the desert lake body is extracted using medium spatial resolution remote sensing images, there are many mixed pixels that could affect the accuracy near the boundaries between the land and water. Therefore, it is necessary to un-mix the pixels to estimate the percentage of water, subsequently providing the foundation for water boundary mapping at the sub-pixel level (Lai et al. 2019). In this paper, we use the dimidiate pixel (DP) model to analyze mixed pixels and calculate water area proportion based on the normalized difference water index (NDWI).

- (1) The NDWI was proposed by McFeeter in 1996. It is based on the spectral characteristics of water and surrounding vegetation in the near-infrared and green bands. The information is used to suppress the vegetation and enhance the water signal to obtain water information in the image. It can be calculated using Eq. (1) (Gu et al. 2020; McFeeter 1996; Wang et al. 2017; Xu 2005):

$$\text{NDWI} = (G - \text{NIR}) / (G + \text{NIR}) \quad (1)$$

where G and NIR are the values of green band and near-infrared band respectively.

- (2) Dimidiate pixel (DP) model.

Assuming that the reflectance of each pixel is composed of a water part (R_W) and a land part (R_L), then its value can be expressed as a linear weighted sum of the two parts, as shown in Eq. (2):

$$R = R_W + R_L \quad (2)$$

If the water area proportion in a mixed pixel is f_w , which is the water coverage index of the pixel, then the land part is $1 - f_w$. If the pixel is entirely composed of water, the reflectance can be represented as R_{water} ; if there is no water in the pixel, the reflectance is R_{land} . Therefore, the information contributed by the water part (which is R_W) can be expressed as the product of the pure water end-member reflectance R_{water} and the water coverage index f_w , while R_L can be expressed as the product of the land part reflectance R_{land} and $1 - f_w$, as shown in Eqs. (3) and (4):

$$R_W = f_w * R_{\text{water}} \quad (3)$$

$$R_L = (1 - f_w) * R_{\text{land}} \quad (4)$$

Then, the water coverage index f_w can be calculated using Eq. (5) (Ding and Liu 2020).

$$f_w = (R - R_{\text{land}}) / (R_{\text{water}} - R_{\text{land}}) \quad (5)$$

According to the principle of the DP model, the NDWI value of a pixel is a composition of the water and land parts, so the equation for calculating the water coverage index can be expressed as Eq. (6):

$$f_w = (\text{NDWI} - \text{NDWI}_{\text{land}}) / (\text{NDWI}_{\text{water}} - \text{NDWI}_{\text{land}}) \quad (6)$$

where f_w is the water coverage index in a mixed pixel, and $\text{NDWI}_{\text{water}}$ and $\text{NDWI}_{\text{land}}$ are the NDWI values of a pure water pixel and a pure land pixel, respectively.

3.2 Water coverage index calculation based on fully constrained least squares (FCLS) pixel unmixing model

The linear spectral unmixing model is a common method to solve the problem of mixed pixels in low-resolution remote sensing images. In this approach, the spectrum of a mixed pixel is considered to be a linear combination of various ground object spectra in the instantaneous field of view, as expressed using Eq. (7).

$$R_i = \sum_{j=1}^n f_j * R_{e,i,j} + \varepsilon_i \quad (7)$$

$$\text{s.t. } \sum_{j=1}^n f_j = 1, \quad 0 \leq f_j \leq 1$$

where R_i is the reflectance of band i ; f_j is the percentage of ground of class j in the pixel; $R_{e,i,j}$ is the reflectance of ground of class j in band i ; and ε_i is the error of band i .

Linear spectral unmixing can be considered as a nonlinear optimization problem with the constraints expressed as Eq. (8).

$$F = \min D(S, XF) \tag{8}$$

$$\text{s.t. } \sum_{j=1}^n f_j = 1, \quad 0 \leq f_j \leq 1$$

where $D(S, XF)$ is the objective function representing the distance between the target mixed pixel reflection spectrum S and the estimated spectrum XF (Chang et al. 2003; Kong and Chen 2017)

The water coverage index f_w can be obtained from Eq. (8) using FCLS.

3.3 Sub-pixel position based on the Cellular Automata model

3.3.1 Cellular automata

Cellular automata (CA) refer to dynamic systems defined in a cellular space composed of cells with discrete and finite states, evolving under certain local rules along a discrete time dimension. These systems follow the bottom-to-top strategy for simulating the change of a complex system. The change of each cell's state at the next generation is determined by its initial state and the influence of the neighboring cells around it. Therefore, small changes in local cells will eventually cause substantial changes in the composition, layout, properties and dynamics of the system (Chen et al. 2020; Fisher et al. 2016; Li and Ye 2002; Li and Yen 2005; Luo et al. 2005; Yang 2008).

A CA-based system consists of a set of cells, the cellular space, neighbors and rules. These can be represented with four tuples, as shown in Eq. (9):

$$C_A = (Zn, S, N, f) \tag{9}$$

where C_A is the CA system, Zn denotes the cellular space, S is a set of finite discrete cellular states, N represents the neighboring cell states, and f is a local state transition function that uses the current state of the cell and the states of all its neighbors to determine the evolution of the state.

As the CA is a computational system that performs complex tasks on the basis of simple items, it is used in the fields of geography, society, environment, etc. (Li and Ye 2002; Liu et al. 2012; Yuan and Liao 2005; Zhang et al. 2016).

3.3.2 Lake body optimization in sub-pixel level based on CA model

The original low-resolution pixel is divided into $N \times N$ sub-pixels in order to determine the water distribution in the

mixed pixel. The number of sub-pixels occupied by the water body can be determined through the water coverage index. Subsequently, the spatial distribution of the water body can be estimated based on the CA model. The specific methods are introduced as follows:

- (1) Cellular space: The original low-resolution mixed pixel and its neighboring pixels are divided into a set of sub-pixels that constitute the cellular space. In order to improve operational efficiency, the cells involved in the transition are limited within the operation space, which is set to the scope of the original mixed pixel. Figure 4 shows the division of cellular space.
- (2) Cellular states: The initial state of each cell is determined according to the water coverage index.
- (3) Neighborhood: The Moore neighborhood is adopted in this study.
- (4) Transition rules: First, the CA evolves through the influence of the neighboring cells and its current state; then, the cellular state is calculated via the constraint of water proportion in a mixed pixel. Lastly, the layout of water body cell is optimized based on the spatial association of the cells. The detailed CA evolution is as follows:

I. Cellular state initialization.

The initial state values of a pure water pixel, pure land pixel and mixed pixel are set to 1, 0, and $k \in (0, 1)$ according to the water coverage index, respectively.

II. System evolution.

① Evolution based on the influence of neighboring cells.

The state transition probability of a cell in a mixed pixel is calculated using Eq. (10).

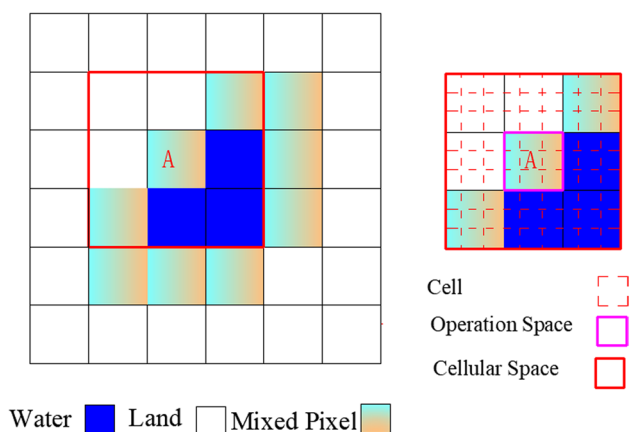


Fig. 4 Schematic diagram of cellular space division

$$S_{t+1}(i,j) = \sum W(m,n) \times S_t(m,n) \quad (10)$$

where $S_{t+1}(i,j)$ represents the state of cell (i,j) at time $t+1$, $S_t(m,n)$ is the state of the neighboring cell (m,n) at time t , and is the weight of the neighboring cell (m,n) , and (m,n) is used as the identifier of the neighborhood.

② Evolution based on the constraints of water coverage in the mixed pixel.

After the first-stage evolution, the cellular state values in the mixed pixel can be differentiated. Subsequently, the number of cells that should be converted to water bodies can be calculated according to the water coverage index and the cellular probabilities in descending order. The calculation is as shown in Eq. (11):

$$N_w = N_k \times f_w \quad (11)$$

where N_w is the number of cells whose state values are set to 1 in the mixed pixel, N_k is the total number of cells in the mixed pixel, and f_w is the water coverage index of the mixed pixel.

③ Optimization of the spatial location.

The cell state can be readjusted to achieve layout optimization according to the spatial connectivity in a mixed pixel. If an exchange of the states of two cells improves the water body pixels' spatial correla-

tion, then the water body's spatial distribution can be optimized.

3.4 Implementation of the model

The water coverage indices of the dimidiate pixel model and FCLS are implemented using the ENVI software with IDL (Interactive Data Language) support, and the CA model is implemented using the ArcGIS software with Python tools. Figure 5 shows the flow chart of the implementation.

3.5 Accuracy evaluation

Accuracy evaluation is an important means to test the reliability of image information extraction method. This is generally achieved by comparing the classification results with ground measured values. A confusion matrix is often established to calculate various classification accuracy metrics. In this study, the lake water boundary extracted from the UAV image is taken as the ground reference to verify the water extraction results obtained using different methods. The commonly used accuracy indices are commission, omission, producer accuracy, user accuracy, overall accuracy and Kappa coefficient. (Pontius Jr and Millones 2011; Li et al. 2021; Xu et al. 2019a, b).

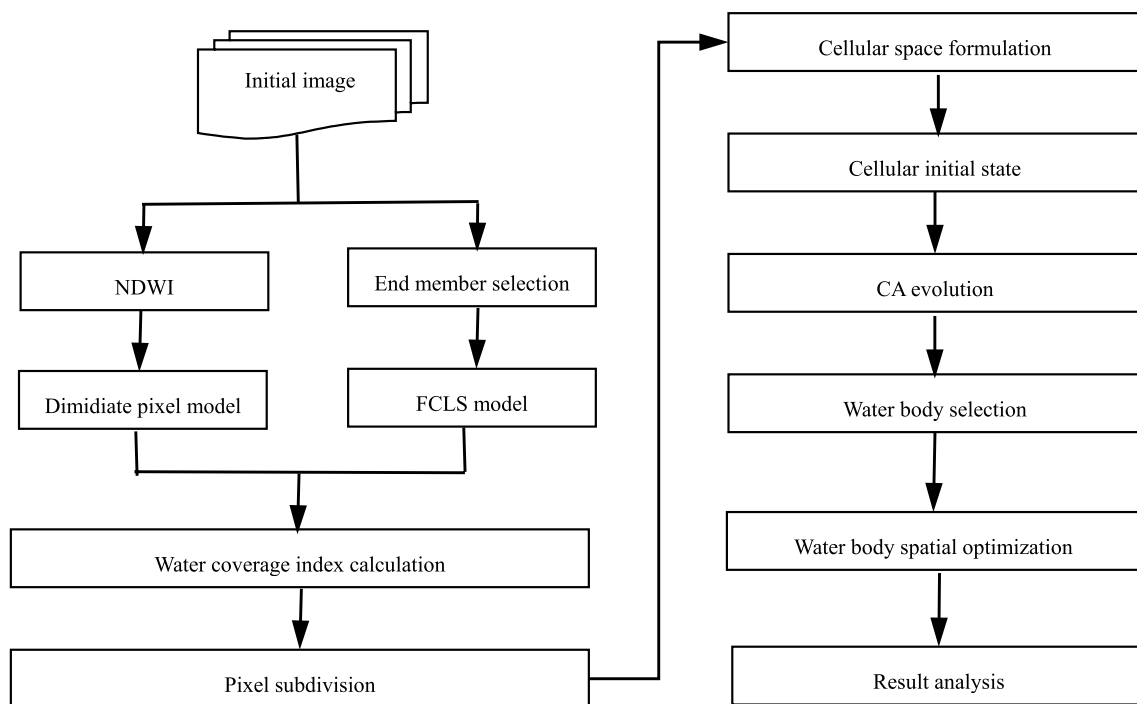


Fig. 5 Flow chart of the study

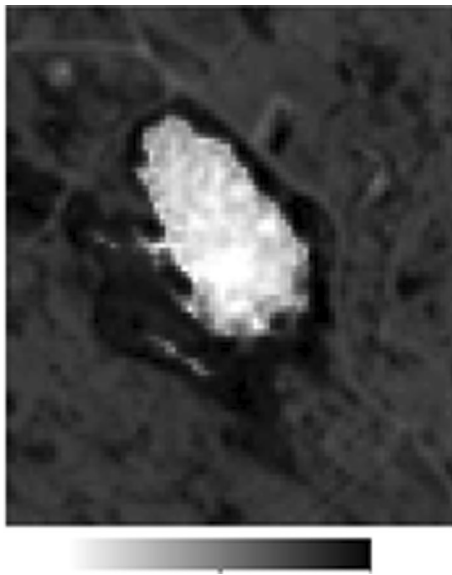


Fig. 6 NDWI Value

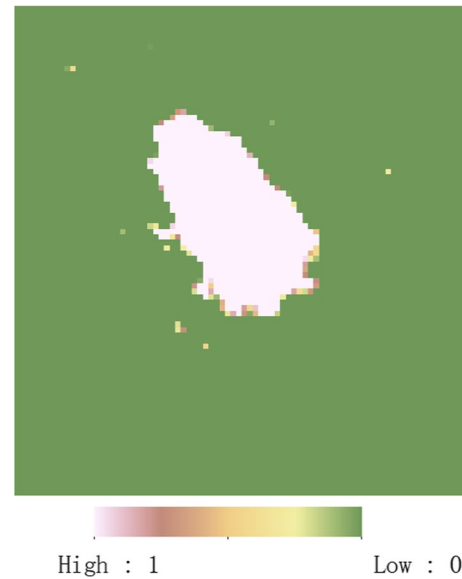


Fig. 7 Distribution of water coverage index

Table 2 Sample information statistics of NDWI

Type	Min	Max	Mean	Std. Dev
Water	-0.0197	0.7241	0.4143	0.1234
Land	-0.6066	-0.1866	-0.3558	0.0625

4 Experimental analyses

4.1 Calculation of water coverage index based on DP model

The NDWI of the study area was calculated according to Eq. (1) and the result is shown in Fig. 6. Water and land samples were selected respectively. The maximum value, minimum value, mean and standard deviation of the NDWI were analyzed (the details are provided in Table 2), and the threshold values for water and land were chosen based on their respective frequency distribution histograms. Subsequently, the distribution of the water coverage index was calculated using Eq. (6) and the result is shown in Fig. 7.

4.2 Calculation of water coverage index using FCLS pixel unmixing model

Depending on the land characteristics of the study area, the land cover was classified into three types, namely

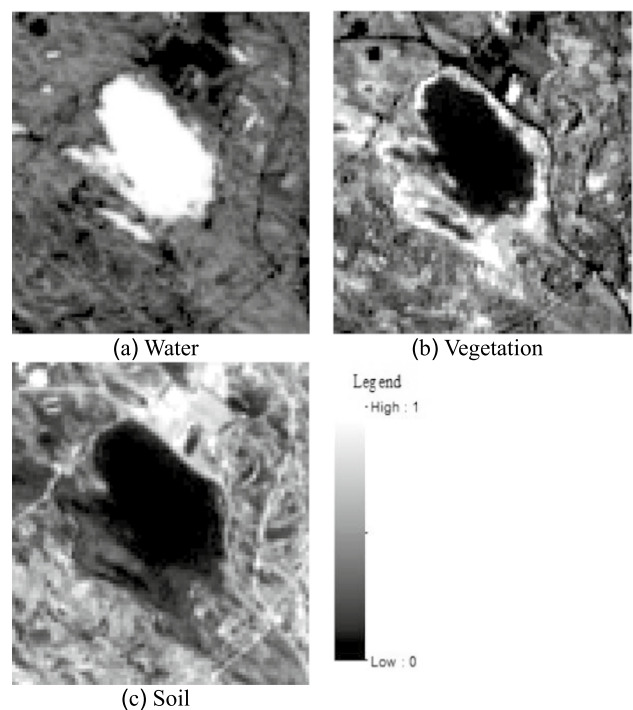


Fig. 8 Coverage index distribution for different land types

vegetation, water and soil land. Then, the pure end elements were selected to calculate the coverage index of the land type using the FCLS tool provided by ENVI. The results are shown in Fig. 8.

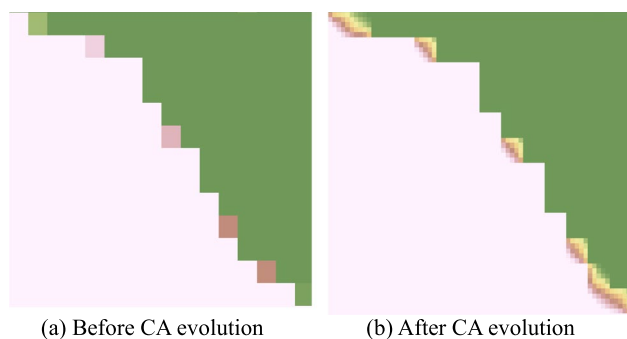


Fig. 9 Local details about the mixed pixel

4.3 CA simulation

4.3.1 CA Model Construction

In order to facilitate the division of the cellular spaces and reduce the error of data processing, the size of the CA is recommended to be an integer division of the resolution for segmentation. So, the water coverage index image of 10 m spatial resolution was subdivided into 2 m spatial resolution in ArcGIS for CA generation using the nearest neighbor method, which does not change the values of the cells.

The neighborhood was set to 3×3 and the weight of the neighborhood cells was assigned based on the distance to the central cell according to the following rules.

The weight value of central cell shall be the largest because it will contribute the most information in next generation the during CA evolution. The weight value of cells that adjoin the central cell with a edge shall be moderate, while for cells that adjoins the central cell with a point, the weight value shall be the lowest. The sum of all weight values of neighborhood shall be equal to one.

4.3.2 CA simulation

Based on the transition rule given by Eq. (10), the intermediate results after CA evolution are shown in Fig. 9. It can be observed that the cellular state values of the mixed images are strongly correlated with the spatial layout of the water body, and the spatial shape is finer than before CA evolution.

Allocation for the cellular state of the lake body was based on water coverage constraints in a mixed pixel. The number of cellular states of the lake body was determined according to the water coverage in the mixed images, and the value of cellular state was changed to water according to the probabilities sorted in descending order after cell evolution.

Although the proportion of water cells in the mixed pixel can be determined after the previous step, there are a few opening holes or discontinuities in the partial layout of a water body. Therefore, the spatial distribution of water cells

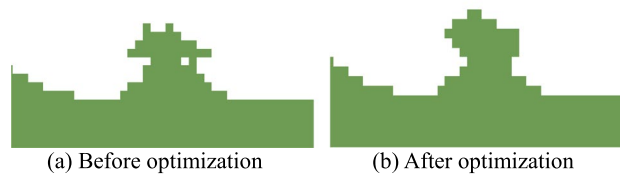


Fig. 10 Spatial optimization for the water cell

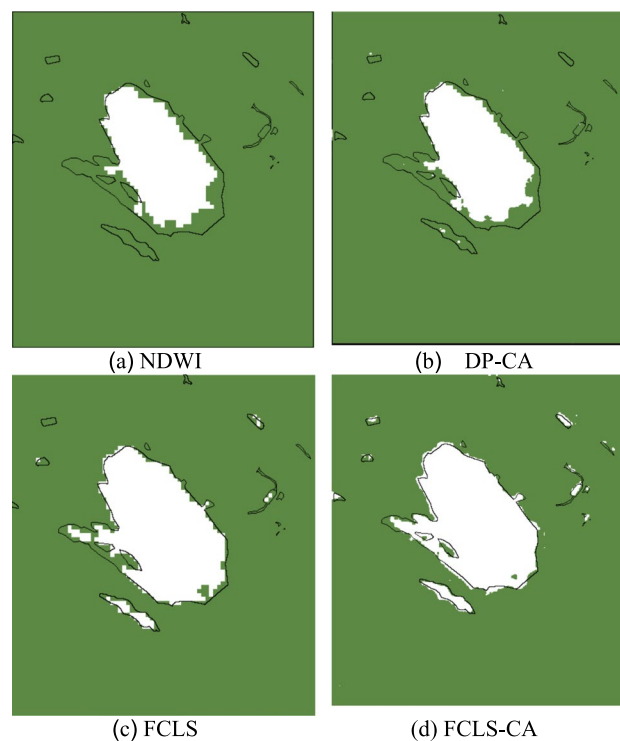


Fig. 11 Comparative analysis of the extracted results

was adjusted based on the spatial correlation. The corresponding results are shown in Fig. 10. It can be observed that the spatial connectivity of water body is improved and the distribution is more logical after CA evolution.

4.4 Accuracy analysis

13 samples about of the lake body were obtained from the UAV image. Next, the extraction results of the lake body using the NDWI, DP-CA, FCLS and FCLS-CA methods were compared with the reference value in Fig. 11. The confusion matrix was calculated by comparing the location and class of each truth pixel with the corresponding location and class in the classification image, respectively.

Subsequently, the commission, omission, producer accuracy, user accuracy, overall accuracy and Kappa coefficient

Table 3 Accuracy evaluation of different water extraction methods

Method	Commission (%)	Omission (%)	Producer accuracy (%)	User accuracy (%)	Overall accuracy (%)	Kappa
NDWI	0.01	33.79	66.21	99.99	95.21	0.7708
DP-CA	0.09	30.36	69.64	99.91	95.65	0.7969
FCLS	7.77	18.89	81.11	92.23	96.14	0.8408
FCLS-CA	11.73	10.60	89.40	88.27	96.81	0.8697

indices were calculated to evaluate the accuracy of different methods. Further details are given in Table 3.

The results show that the FCLS-CA model can identify most water bodies in the study area, and its overall accuracy and Kappa coefficient were higher than those of other methods. This method also achieved a better balance between the indices of commission and omission percentage.

There were some small lakes that could not be identified due to the limited spatial and spectral resolutions of the original remote sensing image.

5 Conclusions

Desert lakes are important wetland resources and hold great significance for maintaining the regional ecological environment. Information extraction relevant to the lakes via remote sensing images is affected by many mixed pixels present in the images. This paper presented a new method to obtain the position and size of water from a mixed pixel in a remote sensing image. Through the use of CA, the distribution of water body can be obtained automatically and the impact of inappropriate threshold value selection, which is a common occurrence in water body index methods, are reduced. The experiments show that the CA model can improve the sub-pixel positioning accuracy for lake bodies in mixed pixel image and improve classification accuracy. Compared with other methods, the FCLS-CA model has a higher accuracy and can identify most water bodies in the study area.

There were some small lakes that could not be accurately identified, so the method still needs further improvement in the future to increase the information extraction accuracy with higher spatial and spectral resolution remote sensing images.

Acknowledgements This work was financially supported by the Shaanxi Province Soft Science Research Program (2022KRM034).

Availability of data and materials Not applicable.

Declarations

Ethics approval and consent to participate Not applicable.

Consent for publication Not applicable.

Competing interests The authors declare that they have no competing interests.

Open Access This article is licensed under a Creative Commons Attribution 4.0 International License, which permits use, sharing, adaptation, distribution and reproduction in any medium or format, as long as you give appropriate credit to the original author(s) and the source, provide a link to the Creative Commons licence, and indicate if changes were made. The images or other third party material in this article are included in the article's Creative Commons licence, unless indicated otherwise in a credit line to the material. If material is not included in the article's Creative Commons licence and your intended use is not permitted by statutory regulation or exceeds the permitted use, you will need to obtain permission directly from the copyright holder. To view a copy of this licence, visit <http://creativecommons.org/licenses/by/4.0/>.

References

- Chang CI, Ren H, Chang CC, D'Amico F, Jensen JO (2003) Subpixel target size estimation for remotely sensed imagery. *IEEE Trans Geosci Remote Sens* 42(46):1309–1320
- Chen XX, Vierling L (2006) Spectral mixture analyses of hyper-spectral data acquired using a tethered balloon. *Remote Sens Environ* 103(103):338–350
- Chen J, Ma L, Chen XH, Rao YH (2016) Research progress of spectral mixture analysis. *J Remote Sens* 20(25):1102–1109
- Chen QJ, Li JY, Hou EK (2020) Dynamic simulation for the process of mining subsidence based on cellular automata model. *Open Geosci* 12(11):832–839
- Cui L, Du HQ, Zhou GM, Li XJ, Mao FJ, Xu XJ, Fan WL, Li YG, Zhu ED, Liu TY, Xing LQ (2019) Combination of decision tree and mixed pixel decomposition for extracting bamboo forest information in China. *J Remote Sens* 23(21):166–176
- Ding PF, Liu HH (2020) Improved water body index extraction method based on dimidiate pixel model. *Henan Sci* 8(10):1625–1632
- Fan WY, Hu BX, Miller J (2009) Comparative study between a new nonlinear model and common linear model for analysing laboratory simulated forest hyperspectral data. *Int J Remote Sens* 30(11):2951–2962
- Feng YJ, Han Z (2012) Cellular automata approach to extract shoreline from remote sensing imageries and its application. *J Image Graph* 17(03):441–446
- Feyisa GL, Meilby H, Fensholt R, Proud SR (2014) Automated water extraction index: a new technique for surface water mapping using landsat imagery. *Remote Sens Environ* 140:25–36
- Fisher A, Flood N, Danaher T (2016) Comparing Landsat water index methods for automated water classification in eastern Australia. *Remote Sens Environ* 175:167–182
- Gao H, Dai ZY (2020) Simulation of water pollution dispersion based on Improved cellular automata. *J Geomat* 45(6):138–140

- Gu JH, Xue HZ, Dong GT, Cheng JH (2020) Applicability analysis of NDWI for drought monitoring in Henan Province. *Agric Res Arid Areas* 38(36):209–217
- Jiang CY, Li MC, Liu YX (2011) Full-automatic method for coastal water Information extraction from remote sensing image. *Acta Geodaetica Cartographica Sinica* 40(43):332–337
- Kong MM, Chen DS (2017) Reservoir water area extraction and monitoring using pixel unmixing. *J Huaqiao Univ (nat Sci)* 38(03):385–390
- Lai PY, Chen HN, Huang C (2019) Study on the suitability of dimidiate pixel model in surface water detection of MODIS at sub-pixel level. *J Geomat* 44(46):56–59
- Li X, Ye JA (2002) Integration of principal components analysis and cellular automata for spatial decision making and urban simulation. *Sci China Ser D Earth Sci* 6:521–529
- Li X, Yen A (2005) Knowledge discovery for geographical. *Cell Automata Sci China Ser D Earth Sci* 48(10):1758–1767
- Li WB, Yu CY, Zhang QW, Cao B (2008) Research on water area estimation based on normalization index. *Yangtze River* 39(32):11–12
- Li H, Wang YP, Li Y, Wang XF (2009) Unmixing of remote sensing images based on support vector machines and pairwise coupling. *Acta Geodaetica Cartographica Sinica* 38(34):318–323
- Li XJ, Lv H, Li YM, Wang Y, Zhang J, Pang HZ (2015) Modification of cellular automata (CA) used in sub-pixel mapping. *Remote Sens Technol Appl* 30(6):1206–1214
- Li H, Zhang JQ, Cao Y, Wang XF (2016) Nonlinear spectral unmixing for optimizing per-pixel endmember sets. *Acta Geod Cartogr Sinica* 45(41):80–86
- Li D, Wu BS, Chen BW, Xue Y, Zhang Y (2020) Review of water body information extraction based on satellite remote sensing. *J Tsinghua Univ (sci Technol)* 60(62):147–161
- Li XY, Fan H, Xu L, Han ZH, Wang FF, Xie HY (2021) Classification evaluation and visualization analysis of remote sensing images—take the area around the Pingmei mining area in Pingdingshan city as an example. *Seismol Geomagn Observ and Res* 42(42):72–80
- Liu RJ (2020) Research on the effect of extracting the water body of Miyun Reservoir based on different methods of multi-source data. *Land Resour Inform* 3:50–57
- Liu LF, Wang B, Zhang LM (2008) Decomposition of mixed pixels based on self-organizing map and fuzzy membership. *J Comput Aided Des Comput Graph* 20(10):1307–1315
- Liu M, Zhang SL, Pan X (2012) Simulation of urban digital evolution based on raster geographic data and cellular automata. *J Changchun Inst Technol (soc Sci Edn)* 13(11):108–110
- Liu Y, Yue H, Wang TL (2017) Dynamic Change of Land Use/Cover and Spatio-temporal Evolution of Landscape Pattern in Hongjiannao Region During 1990–2015. *Bull Soil Water Conserv* 37(35):224–230
- Luo P, Geng JJ, Li MC, Li S (2005) Mechanism of simulating geographic process and extension of cellular automata. *Scientia Geogr Sinica* 25(26):724–730
- Ma YM, Guo CM, Wang Y, Li JP, Tang XL, Chen LW (2018) Remote sensing monitoring on area dynamic change of major water bodies in Western Jilin Province. *Bull Soil Water Conserv* 38(35):249–255
- McFeeter SK (1996) The use of the Normalized Difference Water Index (NDWI) in the delineation of open water features. *Int J Remote Sens* 17(17):1425–1432
- Nie XJ, Gao S, Chen YL, Zhang H (2018) Characteristics of soil erosion and nutrients evolution under coal mining disturbance in Aeolian sand area of Northwest China. *Trans Chin Soc Agric Eng* 34(32):127–134
- Pontius RG Jr, Millones M (2011) Death to Kappa: birth of quantity disagreement and allocation disagreement for accuracy assessment. *Int J Remote Sens* 32(15):4407–4429
- Qiao CJ, Sun J (2020) Remote sensing monitoring of water body area changes in Lugu Lake in recent 45 years. *J Anhui Agric Sci* 48(47):95–99
- Su LF, Li ZX, Gao F, Yu M (2021) A review of remote sensing image water extraction. *Remote Sens Land Resour* 33(31):39–19
- Wang XH, Guo JM, Jia BJ, Zhang YK (2008) Mixed pixels classification of remote sensing images based on Cellular Automata. *Acta Geod Cartogr Sinica* 37(31):42–48
- Wang SJ, Cao X, Li HY, Li QY, Hang X, Wang JJ (2017) Air route network optimization in fragmented airspace based on cellular automata. *Electron Electr Eng Control* 30(33):1184–1195
- Wang DZ, Wang SM, Huang C (2019a) Comparison of Sentinel-2 imagery with Landsat8 imagery for surface water extraction using four common water indexes. *Remote Sens Land Resour* 31(33):157–165
- Wang Z, Yu JK, Lu YG (2019b) Research of the application of remote sensing technology in monitoring water pollution caused by coal suspended matter in typical coal mining areas of Western China. *J Ecol Rural Environ* 35(34):538–544
- Wang QM, Dong SN, Wang WK, Wang H (2020) Effects of high intensive vegetation restoration on groundwater recharge in ecologically fragile mining area. *J China Coal Soc* 45(49):3245–3252
- Wu CS (2004) Normalized spectral mixture analysis for monitoring urban composition using ETM+ imagery. *Remote Sens Environ* 93(94):480–492
- Xu HQ (2005) A study on information extraction of water body with the modified normalized difference water index (MNDWI). *J Remote Sens* 9(5):589–595
- Xu DL, Ding JN, Wu YQ (2019a) Lake Area Change in the Mu Us Desert in 1989–2014. *J Desert Res* 39(36):40–47
- Xu H, Pan P, Yang W, Ouyang XZ, Ning JK, Shao JF, Li Q (2019b) Classification and accuracy evaluation of forest resources based on multi-source remote sensing image. *Acta Agric Univ Jiangxiensis (nat Sci Edn)* 41(44):751–760
- Yang QS (2008) Dynamic transition rules for Geographical Cellular Automata. *Acta Sci Nat Univ Sunyatseni* 47(44):122–127
- Yang GP, Zhou X, Yu XC, Chen W (2010) Relevance vector machine for hyperspectral imagery unmixing. *Acta Electron Sin* 38(12):2751–2756
- Yuan Q, Liao HS (2005) A software based on Cellular Automata used to simulate time and space dynamic change in Geography. *J Nanjing Univ (nat Sci)* 41(z41):857–861
- Zhang RH, Zhao RL, Wu ZG (2016) Urban geosimulation based on ensemble learning and Cellular Automata. *J South China Normal Univ (nat Sci Edn)* 48(41):101–107
- Zhang HN, Wen XP, Xu JL, Luo DY, Li JB (2019) Influence factors of decomposition precision of mixed-pixels based on CLSMM. *Remote Sens Inf* 34(33):48–53
- Zhang B, Li JS, Shen Q, Wu YH, Zhang FF, Wang SL, Yao Y, Guo LN, Yin ZY (2021a) Recent research progress on long time series and large scale optical remote sensing of inland water. *J Remote Sens* 25(21):37–52
- Zhang Q, Feng ZM, Chen P (2021b) The comparison of methods for extracting water body from Glacier Barrier Lake by GF-1 satellite remote sensing images. *Geom Spat Inf Technol* 44(41):17–19
- Zhang L, Han XZ, Wen FZ, Qiu ZF (2022) Comparison of water information extraction algorithms based on sentinel-2A MSI. *Data Laser Optoelectron Progress* 59(12):505–515

Zheng S, Wang L, Liu CS, Liang LL, Chen GF (2021) Water environment quality characteristics and multivariate statistical analysis of lakes in mu us sandy land of ordos. *Water Resour Hydropower Eng* 52(55):129–138

Zhou Y, Dong JW (2019) Review on monitoring open surface water body using remote sensing. *J Geo Inf Sci* 21(11):1768–1778

Zhou Y, Zhou WQ, Wang SX, Zhang B (2004) Applications of remote sensing techniques to inland water quality monitoring. *Adv Water Sci* 15(13):312–317

Publisher's Note Springer Nature remains neutral with regard to jurisdictional claims in published maps and institutional affiliations.